國立臺灣大學理學院大氣科學系

碩士論文

Department of Atmospheric Sciences

College of Science

National Taiwan University

Master Thesis

積雲參數化中對流質量通量之人為就地補償之效應
Effects of Artificial Local Compensation of Convective
Mass Flux in Cumulus Parameterization

王珩

Hing Ong

指導教授：郭鴻基 博士、吳健銘 博士

Advisor: Hung-Chi Kuo, Ph.D., Chien-Ming Wu, Ph.D.

中華民國 105 年 6 月

June 2016

謝辭

感謝指導教授郭鴻基老師，那自由開放的態度、實事求是的精神，是我的榜樣，且教導我從簡單的模式認識大氣動力系統，使我受到潛移默化，終能以更廣闊的觀點思考本研究中的問題。

感謝共同指導教授吳健銘老師，在我對於研究徬徨無助的時候伸出援手，且經常抱持懷疑的態度，使我能夠突破盲點，不斷反思，終能把本研究做得更加深刻。

感謝考試委員王懌琪博士，在口試中提出新的問題以及專業的意見。感謝楊憶婷、徐驊、尤虹叡、陳郁涵、程維毅、許天耀、謝宜桓、孫既仁、吳舜楠、曾開治…等學長姊們，王立中、陳政友、吳佳瑩、陳逸昌、郭威鎮、黃冠捷、陳勇志、曾弘毅…等同學們，陳映如、黃建彰…等學弟妹們，以及親愛的母親平時的討論或最後的校稿，使我能把本研究做得更加完善。

感謝親人、朋友們的關心鼓勵，使我能健康快樂地度過碩士班生涯。

i

摘要

　　本研究旨在對積雲參數化中的對流質量通量，比較人為就地補償與模式動力補償的異同。本研究使用天氣研究與預報模式(the Weather Research and Forecasting Model, WRF)對以下兩個方面比較，一為對水平解析度的依賴性，二為在熱帶氣旋模擬中的效應。使用模式動力補償的積雲參數化方案稱為混成質量通量積雲參數化方案(hybrid mass flux cumulus schemes, HYMACSs)，它們將次網格質量通量輻合或輻散視同參數化質量源或匯來處理。只要在非靜力平衡且完全可壓縮模式中加入這些質量源或匯，模式動力就能解析質量補償運動。質量補償實驗的結果證實，對 3 公里到 27 公里的水平解析度來說，就地補償比動力補償更敏感。『背著跑』實驗的結果證明，在 9 公里解析度使用 Kain-Fritsch 方案(KF)模擬熱帶氣旋，就地補償導致暖化與低層乾化並可使海平面氣壓深化與降水強化。『各自跑』實驗的結果暗示混成質量通量 KF 可以減少在 9 公里解析度使用 KF 模擬高估熱帶氣旋強度的傾向，不過此結果有氣旋尺度與積雲尺度過程之非線性交互作用所造成的不確定性。我們得出此結論：在非靜力平衡且完全可壓縮模式中創制積雲參數化時，動力補償比就地補償更符合自然。另外討論消除就地補償對整合性積雲參數化的重要性。

・　在非靜力平衡且完全可壓縮模式中創制積雲參數化時，動力補償比就地補償更符合自然。

・　對水平解析度來說，就地補償比動力補償更敏感。

・　就地補償導致暖化與低層乾化並可使海平面氣壓深化與降水強化。

關鍵詞：非靜力平衡且完全可壓縮模式、質量補償、積雲參數化、熱帶氣旋模擬

Abstract

In this study, cumulus parameterization schemes with artificial local compensation of convective mass flux are compared with hybrid mass flux cumulus schemes (HYMACSs), implementing dynamic compensation of that, with the Weather Research and Forecasting Model (WRF) in terms of the dependence on the horizontal resolution and the effects in tropical cyclone simulations. HYMACSs treat subgrid-scale mass flux convergence or divergence as subgrid-scale mass sources or sinks. When the mass sources or sinks are introduced to the mass continuity equation in a nonhydrostatic fully compressible model, the model dynamics would resolve the mass-compensating motion. The results of the mass compensation experiment corroborate that the local compensation is more sensitive than the dynamic compensation to the horizontal resolution between 3 and 27 km. The results of the piggyback experiment substantiate that the local compensation in the Kain-Fritsch scheme (KF) causes warming and low-level drying and could lead to sea level pressure deepening and precipitation strengthening at 9 km resolution in tropical cyclone simulations. With uncertainty due to the nonlinear interaction between cyclone-scale and cumulus-scale processes, the results of the fully coupled experiment imply that the hybrid mass flux KF (HY) could reduce the tendency of KF to overestimate the intensity of simulated tropical cyclones at 9 km

resolution. We conclude that the dynamic compensation is more realistic than the local compensation when formulating cumulus schemes in nonhydrostatic fully compressible models. In addition, the importance of the elimination of the local compensation for the unified cumulus parameterization problem is discussed.

- The dynamic compensation is more realistic than the local compensation when formulating cumulus schemes in nonhydrostatic fully compressible models

- The local compensation is more sensitive than the dynamic compensation to the horizontal resolution

- The local compensation causes warming and low-level drying and could lead to sea level pressure deepening and precipitation strengthening

Keywords: Nonhydrostatic fully compressible model, Mass compensation, Cumulus parameterization, Tropical Cyclone Simulation

目錄

圖目錄

表目錄

表目錄

1. Introduction

Cumulus parameterization embodies scientists' knowledge of the interaction between the vertically penetrating convective drafts and the embedding mass-compensating environment. For example, understanding the nature in which the fractional area covered by the convective drafts in the environment is negligible, previous studies [*Arakawa and Wu*, 2013; *Arakawa et al.*, 2011; *Molinari and Dudek*, 1992] concluded the dependence of the representation of cumulus convection on the horizontal resolution in the following. For the horizontal resolution at 25 km or coarser, where the environment should not be too much wider than the grid cell, conventional cumulus schemes with the grid-scale variables being equal to the environmental ones are used to represent the effects of the subgrid-scale cumulus convection on the grid-scale dynamics. On the other hand, for the horizontal resolution at 3 km or finer, where the convective drafts should be much more resolvable than not, explicit schemes without any cumulus parameterization are used to resolve cumulus convection. However, for the horizontal resolution between those, the so-called gray zone, neither the explicit schemes nor the conventional cumulus schemes are reasonable approaches; the former delay and strengthen the cumulus convection, and the latter double count the effects of cumulus convection. Hence, *Arakawa et al.* [2011] initiated the unified cumulus parameterization problem to reduce the dependence of the representation of cumulus convection on the horizontal resolution.
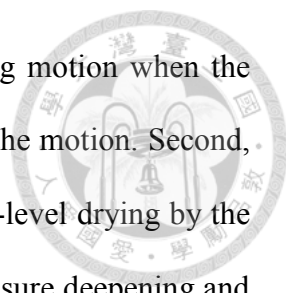
The dependence on the horizontal resolution could be caused by treating the grid cell as the environment, implying two artificial assumptions; one is the neglect of σ, the fractional area covered by the convective drafts in the grid cell, and the other is the local compensation of convective mass flux in the environment. Thus, the unified cumulus

1

parameterization problem might be approached by eliminating those assumptions. Eliminating the neglect of σ has been regarded as a key to the unified cumulus parameterization problem, so new closure assumptions considering σ has been proposed [*Arakawa and Wu*, 2013; *Grell and Freitas*, 2014; *Park*, 2014; *Wu and Arakawa*, 2014; *Zheng et al.*, 2015]. However, eliminating the local compensation has not been well studied, so it is the intention of this research.

Knowing that the mass-compensating motion induced by the subgrid-scale processes could be resolved by the grid-scale dynamics, *Kain and Fritsch* [1993] suggested using the dynamic compensation of convective mass flux instead of the local compensation. Realizing this, *Kuell et al.* [2007] proposed hybrid mass flux cumulus schemes (HYMACSs), which treat subgrid-scale mass flux convergence or divergence as subgrid-scale mass sources or sinks. Then, the mass sources or sinks introduced to the mass continuity equation in a nonhydrostatic fully compressible model would induce perturbation pressure driving the mass-compensating motion. In Figure 1.1, the schematic diagrams for HYMACSs are depicted. *Kuell et al.* [2007] showed that the mass-compensating motion seems not sensitive to the horizontal resolution. Furthermore, *Kuell and Bott* [2008] derived a particular formulation of HYMACSs which yields realistic results in terms of the spatial distribution of precipitation in an idealized simulation of sea breeze circulation initiating convection.

In spite of those studies, a general formulation of HYMACSs for unifying cumulus parameterization has not been derived, and general effects of the local compensation have not been examined. In this study, a general formulation is derived, and two hypotheses about the effects are tested. First, the local compensation could be more sensitive than the dynamic compensation to the horizontal resolution because the

size of a grid column could affect the strength of the compensating motion when the motion is confined in the column; the smaller the size, the stronger the motion. Second, schemes with the local compensation could cause warming and low-level drying by the local compensating subsidence, and they might lead to sea level pressure deepening and precipitation strengthening by inducing a circulation change.

To verify those hypotheses, the local compensation and the dynamic compensation should be compared while all other conditions, especially subgrid-scale mass flux convergence or divergence due to convective drafts, are controlled. The conditions could be prescribed or predicted. In this study, for experiments in which the conditions are predicted, the Kain-Fritsch scheme (KF) [*Kain*, 2004; *Kain and Fritsch*, 1990; 1993] in the Weather Research and Forecasting Model (WRF) [*Skamarock et al.*, 2008], with the local compensation, should be compared with the hybrid mass flux KF (HY), with the dynamic compensation.

KF is chosen because a tendency of KF at 9 km resolution to overestimate the intensity of simulated tropical cyclones is found in previous studies [*Chandrasekar and Balaji*, 2012; *Haghroosta et al.*, 2014; *Sing and Mandal*, 2014; *Srinivas et al.*, 2007; *Sun et al.*, 2013]. In this study, it is conjectured that the local compensation may be a cause of the tendency. In addition, the deterministic nature of cumulus convection in tropical cyclone simulations might hint about the role of cumulus parameterization of gray zone resolution. Therefore, idealized tropical cyclone simulations at 9 km resolution in WRF are studied.

In section 2, an ensemble average continuity equation set, a general formulation of HYMACSs and the particular closure of HY and KF are derived. In section 3, the mass compensation experiment, the piggyback experiment, and the fully coupled experiment

are designed for testing the first hypothesis, the second hypothesis, and the conjecture, respectively. In section 4, the results of the experiments are discussed. In section 5, conclusions are presented, and the importance of the elimination of the local compensation for the unified cumulus parameterization problem is discussed.
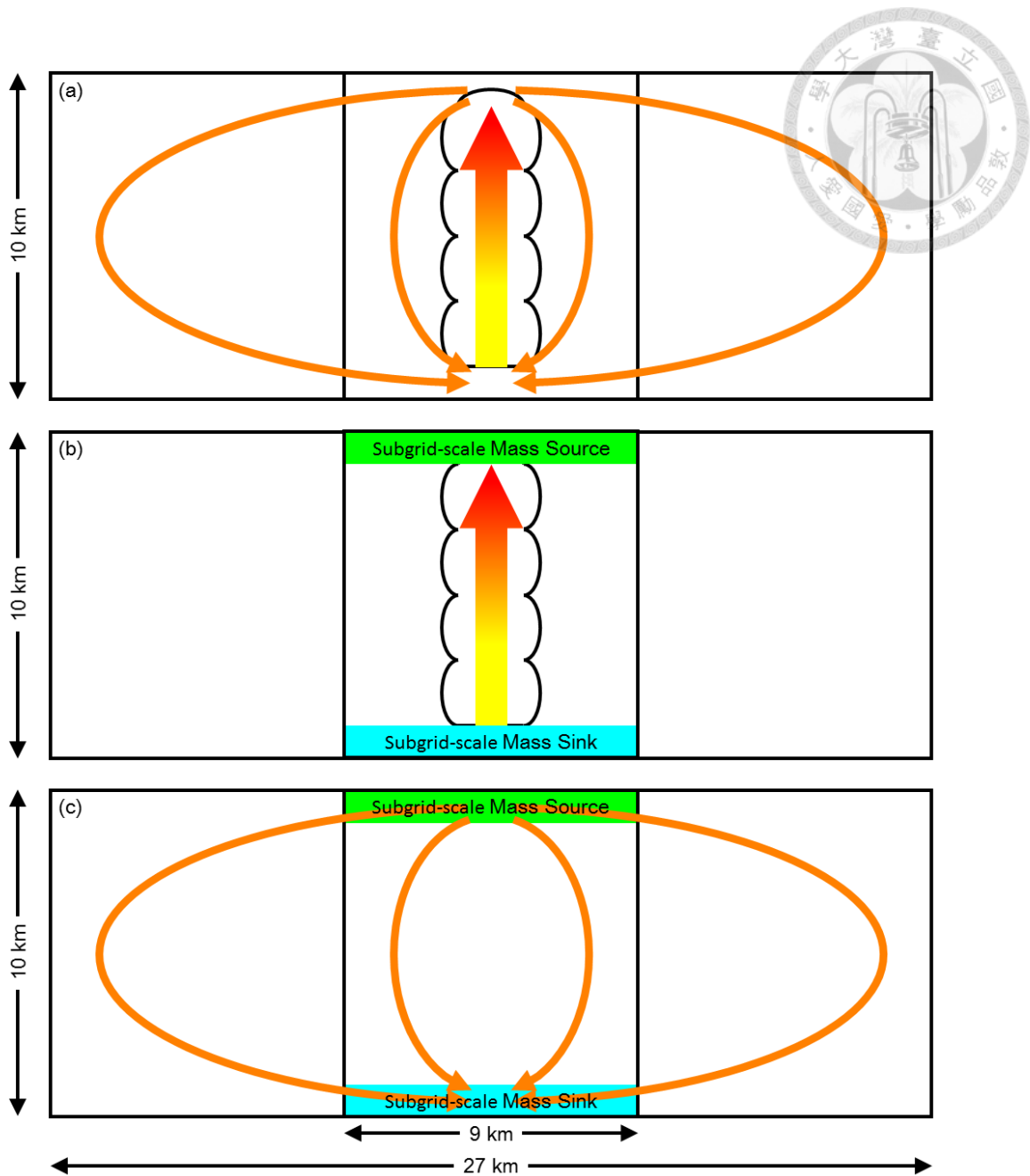
Figure 1.1. The schematic vertical cross sections for HYMACSs are depicted as follows: (a), the natural scale of a convective draft and a mass-compensating environment compared with the size of grid columns; (b), how a grid column treats subgrid-scale mass convergence or divergence; and (c), how grid-scale dynamics respond to the subgrid-scale mass source or sink.

2. Scheme Formulation

2.1. An Ensemble Average Continuity Equation Set

The conservation laws of the fluid dynamics are described by a continuity equation set:

$$\frac{\partial \rho\psi}{\partial t} + \nabla \cdot \rho\psi\mathbf{V} = \rho\dot{\psi}, \tag{1}$$

where the variables are defined as follows: ρ, mass density; ψ, unity or an intensive quantity; $\mathbf{V}$, three-dimensional vector of velocity; and $\dot{\psi}$, total time derivative of ψ. If ψ is unity, three-dimensional vector of velocity, specific enthalpy, and specific moisture contents, equation (1) would be a nonhydrostatic fully compressible continuity equation set composed of the following density as prognostic variables: mass, momentum, enthalpy, and moisture contents, respectively. With respect to the prognostic variables, equation (1) means that the local tendency plus the flux density divergence equals to the density of sources or sinks. Diagnostic equations parameterizing the density of sources or sinks would close the equation set.

However, owing to turbulence, it is more pragmatic to describe the ensemble average components of the variables instead of the total of those. Accordingly, the variables in equation (1) are decomposed into the ensemble average components and the ensemble deviation components:

$$\frac{\partial}{\partial t}[\overline{\rho\psi} + (\rho\psi)'] + \nabla \cdot [\overline{\rho\psi} + (\rho\psi)'][\overline{\mathbf{V}} + \mathbf{V}'] = [\bar{\rho} + \rho']\left[\bar{\dot{\psi}} + \dot{\psi}'\right], \tag{2}$$

where the over bars and the primes denote the average and the deviation, respectively. Then, equation (2) is ensemble averaged, yielding an ensemble average continuity equation set:

$$\frac{\partial \overline{\rho\psi}}{\partial t} + \nabla \cdot \overline{\rho\psi}\overline{V} - \bar{\rho}\overline{\psi} = \overline{\rho'\dot{\psi}'} - \overline{\nabla \cdot (\rho\psi)'V'}, \tag{3}$$

For discrete model dynamics, the ensemble-spatial-temporal average approximation is used; that is, ensemble average is resolvable-scale average while ensemble deviation is unresolvable. Hence, turbulence parameterization represents the effects of unresolvable turbulent flow, such as cumulus parameterization represents those of the subgrid-scale convective drafts. Equation (3) is similar to equation (1). Yet it describes the ensemble average components of the prognostic variables and has a residual term on the right hand side, indicating the subgrid-scale sources or sinks of ψ (SSS$_\psi$). For example, when ψ is unity, $\overline{-\nabla \cdot \rho'V'}$, *the subgrid-scale mass flux convergence or divergence, is the subgrid-scale mass sources or sinks*. In order to close the equation set, SSS$_\psi$ must be diagnosed by turbulence parameterization.

Note that the isobaric layers could be lifted or lowered by subgrid-scale mass sources or sinks. The hydrostatic pressure equation is $\Delta\bar{P} + \bar{\rho}\Delta\bar{\varphi} = 0$, where the notations are defined as follows: Δ, difference between isobaric layers; $\bar{P}$, hydrostatic pressure; and $\bar{\varphi}$, geopotential. Taking time derivative to this equation yields $\Delta\frac{d\bar{\varphi}}{dt} = -\frac{1}{\bar{\rho}}\left(\Delta\frac{d\bar{P}}{dt} + \Delta\bar{\varphi}\frac{d\bar{\rho}}{dt}\right)$. With fixed boundary conditions, the change rate of geopotential, or the enhancement of vertical velocity, due to the subgrid-scale processes could be calculated.

2.2 A General Formulation of HYMACSs

Cumulus parameterization is different from other turbulence parameterization since subgrid-scale convective drafts generally penetrate through a grid column, a pile of grid boxes, so one-dimensional plume models are usually used to represent the vertical

7
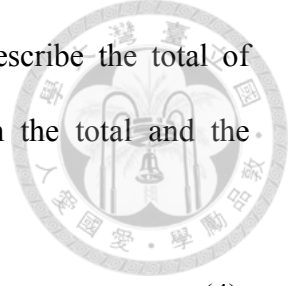
structure of the convective drafts. However, the plume models describe the total of variables, so SSS_ψ must be rewrote into the difference between the total and the ensemble average:

$$\text{SSS}_\psi = \overline{\rho\dot{\psi} - \boldsymbol{\nabla}\cdot\rho\psi\mathbf{V}} - \overline{\bar{\rho}\bar{\dot{\psi}} - \boldsymbol{\nabla}\cdot\overline{\rho\psi}\overline{\mathbf{V}}}, \tag{4}$$

where the two terms are to-be-parameterized by the plume models and to-be-resolved by the model dynamics, respectively. By the ensemble-spatial-temporal average approximation, the ensemble average in equation (4) could be rewrote into spatial average in a grid box:

$$\text{SSS}_\psi \cong \frac{1}{V}\left[\iiint_D (\rho\dot{\psi} - \boldsymbol{\nabla}\cdot\rho\psi\mathbf{V})dV' - \iiint_D \left(\bar{\rho}\bar{\dot{\psi}} - \boldsymbol{\nabla}\cdot\overline{\rho\psi}\overline{\mathbf{V}}\right) dV'\right], \tag{5}$$

where D and V are the grid box and its volume, respectively.

The plume models are inserted into the first integral in equation (5) by decomposing the grid box into a few subgrid columns of convective drafts embedded in a subgrid column of clear sky

$$\text{SSS}_\psi \quad \cong \quad \frac{1}{V}\Sigma_i\left[\iiint_{D_i} (\rho\dot{\psi} - \boldsymbol{\nabla}\cdot\rho\psi\mathbf{V})dV' + \iiint_{\tilde{D}} (\rho\dot{\psi} - \boldsymbol{\nabla}\cdot\rho\psi\mathbf{V})dV' - $$

$$\iiint_D \left(\bar{\rho}\bar{\dot{\psi}} - \boldsymbol{\nabla}\cdot\overline{\rho\psi}\overline{\mathbf{V}}\right) dV'\right], \tag{6}$$

where the subscripts i and the tildes denote the ith subgrid column of convective drafts and the subarid column of clear sky, respectively. *Note that the clear sky is not the environment*; the former is part of a grid box without convective drafts, and the latter is where mass compensating motion occurs which could extend out of a grid box.

As far as the interaction between the convective drafts and the clear sky is concerned, the top-hat profile approximation is used; that is, ψ is spatially homogeneous in each subgrid column. Also, the flux on the boundaries of the subgrid columns is more

8

representative than the flux divergence within the subgrid columns, so the divergence

theorem is applied to the integrals of flux density divergence in equation (6):

$$\text{SSS}_\psi \cong \frac{1}{V}\Big[\sum_i\big(\Psi_i + \varepsilon_i\tilde{\psi} - \delta_i\psi_i - J_{it}\psi_{it} - J_{ib}\psi_{ib}\big) + \big(\widetilde{\Psi} - \sum_i \varepsilon_i\tilde{\psi} + \sum_i \delta_i\psi_i - \widetilde{J_t}\widetilde{\psi_t} -$$

$$\widetilde{J_b}\widetilde{\psi_b}\big) - \big(\overline{\Psi} - \overline{J_t\psi_t} - \overline{J_b\psi_b}\big)\Big], \tag{7}$$

where the variables are defined as follows: Ψ, sources or sinks; ε_i, entrainment rate; δ_i,

detrainment rate; J, outward or inward vertical mass flux; subscript t, upper boundaries;

subscript b, lower boundaries. The three parentheses denote the local tendency of

spatially integrated $\rho\psi$ in the ith convective draft, the clear sky, and the grid box,

respectively. Note that the flux on the lateral boundary of the grid box has been canceled

by that of the clear sky since the convective drafts contribute nothing here. Figure 2.1 is

a schematic diagram for the first two parentheses in equation (7). All terms except sources

or sinks are mass-coupled ψ flux, i.e., the mass flux multiplied by the ψ in the

upstream or on the boundary. Since ε_i is the mass flux from the clear sky to the

convective draft, it is multiplied by $\tilde{\psi}$. Oppositely, δ_i is the mass flux from the

convective draft to the clear sky so is multiplied by ψ_i. Moreover, J is the vertical mass

flux on the boundary so is multiplied by ψ on the boundary.

Equation (7) is a general formulation of HYMACSs. It considers SSS_ψ as the

difference between the total and the ensemble average and treats the total with the

ensemble-spatial-temporal average approximation and the top-hat profile approximation.

Furthermore, considering σ, a weighted average equation, $\overline{A} = \sum_i \sigma_i A_i + (1 - \sum_i \sigma_i)\tilde{A}$

for any variable A, could be applied to every variable with an over bar in equation (7).

On the other hand, the particular formulation of cumulus schemes using one-dimensional

plume models with the local compensation, either neglecting σ [*Arakawa and Schubert*,

1974; *Emanuel*, 1991; *Gregory and Rowntree*, 1990; *Kain and Fritsch*, 1993; *Tiedtke*,

1989; *Zhang and McFarlane*, 1995] or considering σ [*Arakawa and Wu*, 2013; *Grell and Freitas*, 2014; *Park*, 2014; *Wu and Arakawa*, 2014; *Zheng et al.*, 2015], could be derived from equation (7) by confining the subgrid-scale mass sources or sinks term to zero. Thus, treating the subgrid-scale mass sources or sinks term in a parallel manner with the other subgrid-scale sources or sinks terms should simplify those schemes into HYMACSs. In this paper, KF is chosen as an example for the simplification.

2.3 The Particular Closure of HY and KF

In addition to the ensemble-spatial-temporal average approximation and the top-hat profile approximation, before implementing the plume models, KF uses other three assumptions in the following: the steady state, the neglect of σ, and the local compensation. These assumptions are usually used in conventional cumulus schemes but may not be generally applied to the unified cumulus parameterization problem. On the other hand, HY only uses the first two assumptions by eliminating the local compensation assumption.

The steady state assumption means that the convective drafts remain in steady states within a characteristic time of convective adjustment, about 30 minutes. This sets the first parenthesis in equation (7) to zero:

$$\text{SSS}_\psi \cong \frac{1}{V}\left[\left(\widetilde{\Psi} - \sum_i \varepsilon_i \tilde{\psi} + \sum_i \delta_i \psi_i - \widetilde{J_t}\widetilde{\psi_t} - \widetilde{J_b}\widetilde{\psi_b}\right) - \left(\overline{\Psi} - \overline{J_t \psi_t} - \overline{J_b \psi_b}\right)\right], \qquad (8)$$

This assumption may not be a realistic approximation since it stops the convective drafts from changing until the characteristic time is over. However, it is acceptable in this study, as far as a time scale not shorter than the characteristic time is concerned. Note that this assumption also sets that $\varepsilon_i - \delta_i - J_{it} - J_{ib} = 0$ when ψ is unity for any i.

The neglect of σ assumption simplifies the weighted average equation to $\tilde{A} = \bar{A}$, treating the clear sky as the grid box. Applying this to every variable with a tilde in equation (8) yields the particular formulation of HY, with the dynamic compensation:

$$\text{SSS}_\psi \cong \frac{1}{V}\sum_i(-\varepsilon_i\bar{\psi} + \delta_i\psi_i). \tag{9a}$$

which is equivalent to equation (11) and (12) in *Kuell et al.* [2007]. On the other hand, the neglect of σ assumption with the local compensation assumption breaks the parallel of the weighted average equation; $\tilde{J} = \bar{J} - \sum_i J_i$ for mass flux, but $\tilde{A} = \bar{A}$ for any other variable. Applying these to each variable with a tilde in equation (8) yields the particular formulation of KF:

$$\text{SSS}_\psi \cong \frac{1}{V}\sum_i(-\varepsilon_i\bar{\psi} + \delta_i\psi_i + J_{it}\overline{\psi_t} + J_{ib}\overline{\psi_b}), \tag{9b}$$

which is equivalent to equation (16.8) in *Kain and Fritsch* [1993]. Equation (9a) means that SSS_ψ is the average effects of the following mass-coupled ψ flux: $-\varepsilon_i\bar{\psi}$, flux from the clear sky to the convective drafts; $\delta_i\psi_i$, flux from the convective drafts to the clear sky. In addition, equation (9b) has the local compensation terms in the following: $J_{it}\overline{\psi_t}$, downward flux on the upper boundary of the clear sky compensating the convective updrafts, or upward one compensating the convective downdrafts; $J_{ib}\overline{\psi_b}$, flux similar to $J_{it}\overline{\psi_t}$ but on the lower boundary. Note that $\text{SSS}_1 = 0$.

The neglect of σ could not be a realistic approximation when it comes to 9 km horizontal resolution. Why not consider σ in this study? The purpose of this study is to examine the effects of the local compensation, so considering things other than the local compensation in one scheme but not in the other would contaminate the results. Why not use the multiscale KF [*Zheng et al.*, 2015], considering σ, instead of KF for the simplification? The multiscale KF assumes the local compensation, so their assumption replacing the neglect of σ might rely on the assumption of the local compensation. In

essence, implementing the dynamic compensation simplifies the formulation of a cumulus scheme by eliminating the local compensation, but considering σ sophisticate that by replacing the neglect of σ with another assumption.
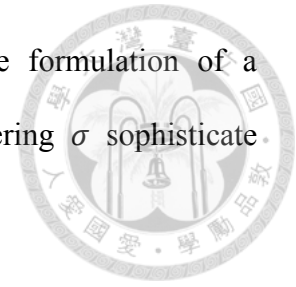
The particular closure of HY and KF is done by two one-dimensional plume models diagnosing ε_i, δ_i, J_{it}, J_{ib}, and ψ_i in equation (9a) and (9b), respectively; one with $i = u$ for convective updrafts, and the other with $i = d$ for convective downdrafts. HY and KF use the same plume models from KF, including the trigger function and the convective available potential energy removal process, but use different formulations for SSS_ψ. HY, with the dynamic compensation, has subgrid-scale mass sources or sinks due to entrainment and detrainment in the convective drafts, which would be compensated with nonhydrostatic fully compressible model dynamics. On the other hand, KF, with the local compensation, has mass compensating flux in the clear sky which offsets the mass sources or sinks due to the convective drafts.
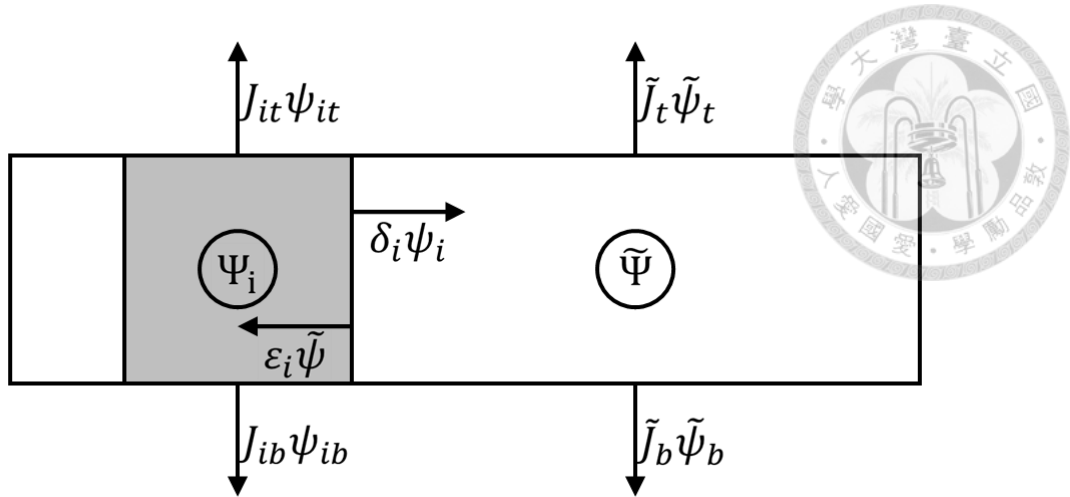
Figure 2.1. The schematic vertical cross section for equation (7). The ith convective draft is filled with gray and is marked with subscripts i while the clear sky is filled with white and is marked with tildes. The circles denote sources or sinks, and the arrows denote mass-coupled ψ flux.
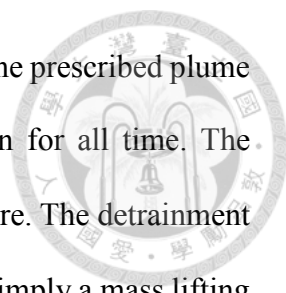
3. Experiment Design

3.1 The Mass Compensation Experiment

The mass compensation experiment is designed to corroborate the first hypothesis in this paper, in which the local compensation could be more sensitive than the dynamic compensation to the horizontal resolution. Therefore, the local compensation should be compared with the dynamic compensation at various resolution while all other conditions, especially subgrid-scale mass sources or sinks due to convective drafts, are controlled. In this experiment, the conditions are prescribed by the settings used in the mass lifting experiments in *Kuell et al.* [2007]. Three horizontal resolution settings, 3, 9, and 27 km are used, representing the fine resolution, the gray zone one, and the coarse one, respectively. Accordingly, six sensitivity tests are listed in Table 3.1.

Those tests are conducted with WRF version 3.7.1 using the nonhydrostatic fully compressible model dynamics. Here are the settings. The large time step is set to the horizontal grid spacing divided by 200 m s^{-1} while the small one is set to the large one divided by 6. The vertical grid spacing is about 1.25 km. The simulation lasts 27 minutes. The domain size is 945 km × 945 km × 25 km. The lateral boundary conditions are periodic. Rayleigh damping is used within the uppermost 5 km. Coriolis parameter is zero. The initial conditions are motionless, horizontally homogeneous, and vertically stratified with the mean hurricane season sounding for the West Indies area. Physical parameterization schemes are turned off except for the cumulus schemes.

In this experiment, cumulus schemes are formulated with equation (9a) and (9b) for the tests of the dynamic compensation and the local compensation, respectively. However, a plume model with a prescribed convective updraft is used instead of the

plume models of KF, which could depend on horizontal resolution. The prescribed plume model is triggered in the grid column at the middle of the domain for all time. The entrainment rate, ε_i, is 4×10^8 kg s^{-1} at the bottom and is zero elsewhere. The detrainment rate, δ_i, is 4×10^8 kg s^{-1} at 10 km height and is zero elsewhere. These imply a mass lifting rate of 4×10^8 kg s^{-1}. The value of ψ_i at any level is equal to that of $\bar{\psi}$ at the level of detrainment. This implies no local tendency of ψ. Hence, the heating rate due to the convective draft is the mass lifting rate times the temperature at the level of entrainment multiplied by the specific entropy difference between the level of detrainment and that of entrainment. Note that the local compensation tests have extra heat sources due to downward flux in the clear sky. Since the mass lifting rate and the local tendency of ψ are constant, the sensitivity of the results to the horizontal resolution could only be caused by the mass compensation processes; either the dynamic compensation or the local compensation.

3.2 The Piggyback Experiment

The piggyback experiment is designed to substantiate the second hypothesis in the paper. In the hypothesis, schemes with the local compensation could cause warming and low-level drying by the local compensating subsidence, and they might lead to sea level pressure deepening and precipitation strengthening by inducing a circulation change. In this experiment, the conditions are predicted by the default settings of idealized tropical cyclone simulation in *Rotunno and Emanuel* [1987]. Predicted conditions are certainly more realistic than prescribed ones but possibly more dependent on the horizontal resolution than those. Thus, as mentioned in section 1, the effects of the local compensation in KF at 9 km resolution in the tropical cyclone simulation are examined. Now here is the problem; how to control the predicted conditions?
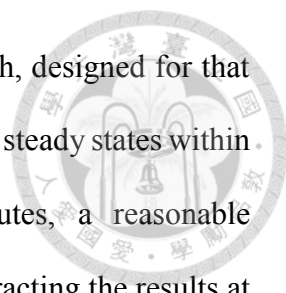
Figure 3.1 is a schematic diagram for the piggyback approach, designed for that problem. Since subgrid-scale convective drafts in HY or KF remain in steady states within a characteristic time of convective adjustment, about 30 minutes, a reasonable approximation to the effects of the local compensation could be subtracting the results at end of a 30-minute simulation with HY from that with KF. In order to examine the effects in various initial conditions, the tropical cyclone simulation is run with KF for five days and is restarted with HY every 30 minutes; that is, the initial conditions of the sensitivity simulations with HY are predicted by a control simulation with KF, as if the sensitivity ones piggyback the control one. In order to reduce the degrees of freedom, the sensitivity simulations are started after two-day spin-up of the control simulation so that the horizontal distribution of cumulus convection is more axisymmetric than not. There are problems when KF piggybacks HY since KF cannot turn off the mass sources and sinks.

The settings of the tropical cyclone simulations follow that in the mass compensation experiment in terms of the time step, vertical grid spacing, lateral boundary conditions, and Rayleigh damping. The horizontal grid spacing is 9 km. The domain size is 5400 km × 5400 km × 25 km. Constant Coriolis parameter at 5×10^{-4} s^{-1} and constant sea surface temperature at 28 $^{\circ}$C are held. The initial conditions of the control simulation follow the ones in the mass compensation experiment by placing a hydrostatic and gradient wind balanced hurricane-like vortex in the middle of the domain with the parameters as follows: outer radius, 412.5 km; radius of maximum wind, 82.5 km; maximum wind speed, 15 m s^{-1}; and depth, 20 km. Physical parameterization schemes are used as follows: microphysics, Kessler [*Kessler*, 1995]; planetary boundary layer, Yonsei University [*Hong et al.*, 2006]; surface layer, MM5 similarity [*Beljaars*, 1995; *Dyer and Hicks*, 1970; *Paulson*, 1970; *Webb*, 1970; *Zhang and Anthes*, 1982]; and radiation, capped Newtonian relaxation [*Rotunno and Emanuel*, 1987].

3.3 The Fully Coupled Experiment

The fully coupled experiment is designed to be more realistic than the piggyback experiment. The control simulation in this experiment uses the explicit scheme at 3 km resolution, which should be more realistic than any scheme at 9 km resolution, while other settings follow that in the piggyback experiment. The control simulation and three sensitivity simulations are listed in Table 3.2.

However, the sensitivity simulations are controlled only initially because the cyclone-scale and the cumulus-scale processes are fully coupled. The nonlinear interaction between the processes makes it uncertain to infer the causality between them from the results. Still, comparing KF9 with NO3 might support whether KF tends to overestimate the intensity of simulated tropical cyclone, and comparing HY9 with KF9 might support whether HY reduces the tendency. Moreover, by comparing NO9 with NO3, the role of cumulus parameterization in tropical cyclone simulations at 9 km resolution could be discussed.

Table 3.1. List of sensitivity tests in the mass compensation experiment.

Horizontal resolution (km)	3	9	27
Local compensation	Lo3	Lo9	Lo27
Dynamic compensation	Dy3	Dy9	Dy27

18
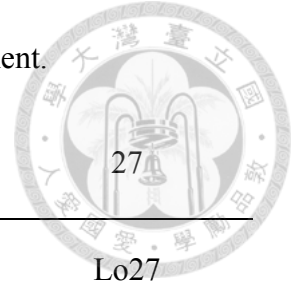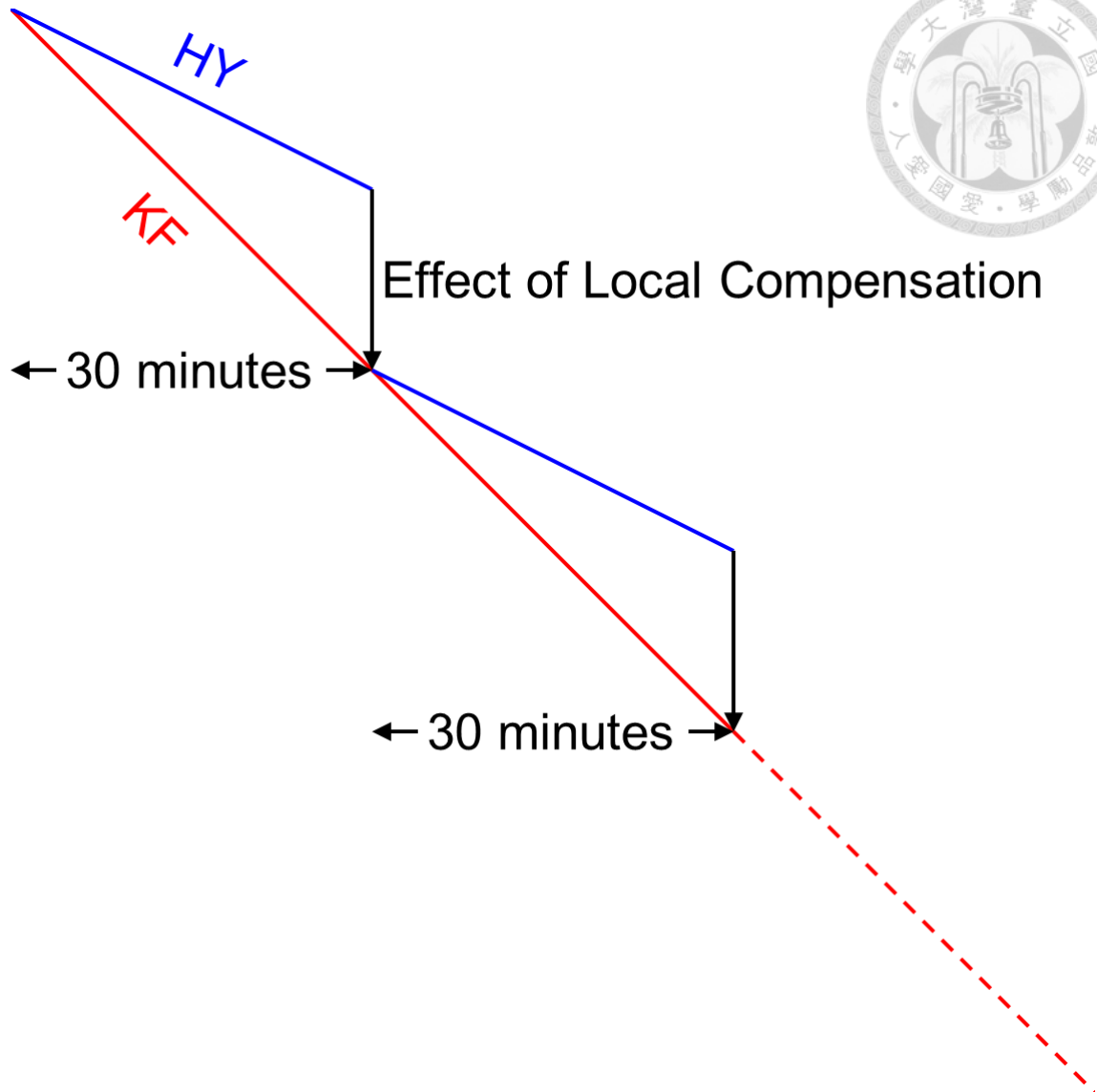
Figure 3.1. The schematic temporal evolution of a variable for the piggyback experiment. The simulation is run with KF, with the local compensation, and is restarted with HY, with the dynamic compensation, every 30 minutes, as if HY piggybacks KF. Subtracting HY from KF could be an approximation to the effect of the local compensation.

Table 3.2. List of simulations in the fully coupled experiment.

Horizontal resolution (km)	3	9 (sensitivity)
Explicit scheme without any cumulus parameterization	NO3 (control)	NO9
Kain-Fritsch scheme (KF)		KF9
Hybrid mass flux Kain-Fritsch scheme (HY)		HY9

20

4 Experiment Results

4.1 The Mass Compensation Experiment

The results of Dy3, Dy9, and Dy27 are comparable with the results of the mass lifting experiments in *Kuell et al.* [2007] in terms of the temporal evolutions of the spatial structures of the momentum fields. Furthermore, in Figure 4.1, the results of Dy3, Dy9, and Dy27 are compared with the results of Lo3, Lo9, and Lo27 in terms of the temporal evolutions of the column mass change, which is the horizontal average of dry air weight per area in the 27 km × 27 km column at the middle of the domain.

In Figure 4.1, all the temporal evolutions of the column mass change are decreasing and oscillating. The decrease is more significant with the local compensation than the dynamic compensation, which should be caused by the extra heat sources due to the local-compensating downward flux in the clear sky. The frequency of the oscillation is independent of the scheme but is dependent on the horizontal resolution. Moreover, for a scheme, the difference between the amplitude of the oscillation at various resolution implies the sensitivity to the horizontal resolution. Though there are various phases of the oscillation, the amplitude at a certain phase could be a proxy for that of the oscillation. For example, at the crest, the difference between the amplitude of Lo27 and Lo3 is seven times larger than that of Dy27 and Dy3, and this could generally apply to other phases.

This indicates that the local compensation is more sensitive than the dynamic compensation to the horizontal resolution in terms of the amplitude of the oscillation of the column mass change. This could be attributed to stronger extra heat sources due to local-compensating downward flux in the clear sky when a finer horizontal resolution is

21

used with the local compensation. Accordingly, the first hypothesis in this paper is corroborated.

4.2 The Piggyback Experiment

First, the results of the control simulation, with KF, are surveyed. The horizontal distribution of total precipitation or subgrid-scale one is concentrated within 216 km from the center of the tropical cyclone and is more axisymmetric than not after the 48th hr of the simulation. Therefore, the domain of scanning reduces to 216 km from the center and from the 48th hr to the 120th hr.

Then, in the domain of scanning, the results of the sensitivity simulation, with HY, subtracted from that of the control simulation, with KF, which are approximately the effects of the local compensation, are examined in terms of dry static energy density, water vapor mixing ratio, radial mass flux, sea level pressure, and precipitation. The temporal averages of those effects would be exceeded by the temporal standard deviation in some regions when a total of three days is taken but would not be exceeded in most regions when a stage of 12 hr is taken except for the center, where subgrid-scale shallow convection in the cumulus schemes occurs sporadically. Hence, the domain of scanning is separated into six stages, and each stage lasts 12 hr.

Furthermore, in each stage, the temporal averages of those effects are scrutinized. Most of the variability could be explained by the first stage and the last stage. The first stage, from the 48th hr to the 60th hr, is called the tropical storm (TS) stage because the maximum 10 m wind speed is from 19.1 m s^{-1} to 30.8 m s^{-1}, and the last stage, from the 108th hr to the 120th hr, is called the typhoon (TY) stage because that is from 49.7 m s^{-1} to 50.0 m s^{-1}. The temporal averages of those effects in the three stages from the 72nd hr

to the 108th hr are similar to those in the TY stage, and those in the stage from 60th hr to 72th hr lies between those of the TS stage and the TY stage. Thus, the following paragraphs describe and interpret the results in the TS stage and the TY stage.

In Figure 4.2, the horizontal distributions of the precipitation in the control simulation are depicted. The subgrid-scale precipitation is calculated by a cumulus scheme while the total precipitation is the sum of the subgrid-scale one and the grid-scale one calculated by a microphysics scheme. Indeed, the distributions are more axisymmetric than not. Furthermore, the precipitation in Figure 5 is scrutinized in the following two paragraphs.

First, the subgrid-scale precipitation and the total precipitation are compared. The former is less than the latter; about three times in the TS stage and about 20 times in the TY stage in terms of the contour which rings. Moreover, the radii of the maxima of the former are about 30 km larger than those of the latter, which determines the eyewall of the tropical cyclone. In general, the subgrid-scale precipitation dominates in the outside of the eyewall while the grid-scale one dominates in the eyewall. This could be attributed to the strength of grid-scale forcing; a weak one could trigger subgrid-scale convection while a strong one could trigger grid-scale convection.

Then, the subgrid-scale precipitation in the TS stage and that in the TY stage are compared. The radius of the maximum azimuthal average of the former is 81.5 km, and that of the latter is 46.2 km. Moreover, the spread of the former is about three times wider than that of the latter, and the maximum of the former is about one-and-one-half times larger than that of the latter in terms of the contour which rings. In general, the subgrid-scale precipitation shrinks while the tropical cyclone intensifies. This could be attributed to the strength of secondary circulation induced by heating due to precipitation in the
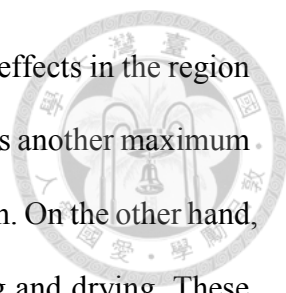
23

eyewall; a stronger circulation could cause more thermodynamic stabilization, inhibiting convection, in the outside of the eyewall.

In Figure 4.3, the subgrid-scale heat sources and sinks with KF and those plus the subgrid-scale potential energy sources and sinks with HY are depicted. Since those with HY are small, KF heats the atmosphere with the local compensation terms in equation (9b), but HY lifts the atmosphere with mass sinks in the cloud base and mass sources in the cloud top. The horizontal distributions of the sources and sinks are generally proportional to those of the subgrid-scale precipitation. The height of the maxima of the sources with KF is lower than that with HY. This could be attributed to the local compensating subsidence with KF. Note that the cyclone-scale circulation is upward and outward following the contour of absolute angular momentum in the free atmosphere.

From Figure 4.4 to Figure 4.8, the temporal averages of the effects of the local compensation in each stage are depicted. As explained in section 3.2, the effects are approximated by subtracting the results in the sensitivity simulations, with the dynamic compensation, from the results in the control simulation, with the local compensation.

In Figure 4.4, warming in terms of dry static energy density due to the local compensation is found in most regions of the tropical cyclone between 300 hPa and the surface. In Figure 4.5, drying in terms of water vapor mixing ratio due to the local compensation is found in most regions of the tropical cyclone in between 700 hPa and the surface. Both warming and drying could be explained by the subgrid-scale local compensating subsidence; since dry static energy normally increase with height throughout the troposphere, but water vapor mixing ratio normally decreases with height in the low level. However, the maxima of both effects are not consistent with the maximum of subgrid-scale processes, and this may imply that the cyclone-scale upward

motion could offset part of both effects. There is a maximum of both effects in the region 30 km outside of the maximum of subgrid-scale processes, and there is another maximum of both effects in the TY stage due to subgrid-scale shallow convection. On the other hand, slight cooling and wetting are found in regions higher than warming and drying. These could be explain by the subgrid-scale cumulus detrainment of cooler and wetter air to the clear sky. Overall, total dry static energy increases in both stages, and total water vapor decreases in the TS stage but remains in the TY stage, implying precipitation strengthening in the TS stage.

In Figure 4.6, the radial mass flux change rate due to the local compensation is depicted. Note that KF in WRF has no subgrid-scale momentum sources or sinks, so this should be the circulation change induced by the local compensating warming. The position of the circulation change is consistent with the local compensating warming. Moreover, the circulation change is weaker in the inside than in the outside, and this asymmetry could be attributed to stronger inertial stability in the inside than in the outside.

The circulation change due to the local compensation could cause other effects which are depicted in the following figures: Figure 4.7, the sea level pressure change; Figure 4.8, the total precipitation change. The circulation change in the TS stage is stronger than in the TY stage, so should those effects be. One may expect that the outward transport of low absolute angular momentum due to the circulation change in the low level could weaken the tangential wind, but this is actually not significant.

In Figure 4.7, sea level pressure deepening due to the local compensation is found in most regions of the tropical cyclone. This could be caused by the strong high-level outflow in the outside of the circulation change, which reduces the mass inside. The
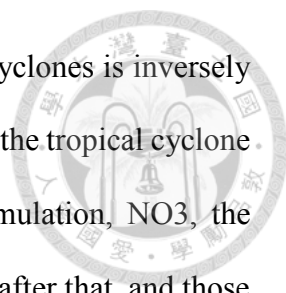
region of the strongest deepening is consistent with the position of the circulation change. As expected, the deepening in the TS stage is more than that in the TY stage.

In Figure 4.8, indeed, in the TS stage, the sum of the total precipitation due to the local compensation increases in the domain. Precisely, the total precipitation increases in the regions where the circulation change converges in the low level, about 30 km outside of the radii of maximum subgrid-scale precipitation, and slightly decreases in other regions. On the other hand, in the TY stage, the total precipitation also increases in those regions but dramatically decreases in the eyewall. This may imply a competition for precipitable water between different regions of the tropical cyclone in the TY stage.

Overall, in comparison to the scheme with the dynamic compensation, HY, the scheme with the local compensation, KF, causes warming and low-level drying, by which a circulation change is induced. Then, the circulation change could cause other effects, such as sea level pressure deepening and a precipitation increase. The maxima of the effects are as follow: warming, 10.0 kJ m^{-3} day^{-1}; low-level drying, -7.5 g kg^{-1} day^{-1}; sea level pressure deepening, -8.0 hPa day^{-1}; and precipitation strengthening, 25.0 mm day^{-1}. Except the precipitation strengthening, all these effects are significantly larger than the natural variability of the tropical cyclone. Accordingly, the second hypothesis in this paper is substantiated with a little uncertainty about the importance of the precipitation strengthening effect.
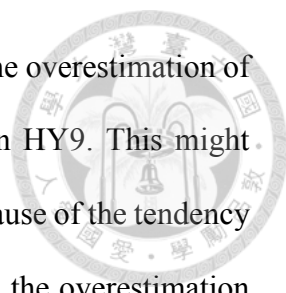
4.3 The Fully Coupled Experiment

The results are depicted as follows: Figure 4.9, the temporal evolutions of the minimum sea level pressure after two-day spin-up; Figure 4.10, the radial distributions of the azimuthal average of the precipitation in the first 60 hr; Figure 4.11, the radial

distributions of those in the last 60 hr. The intensity of the tropical cyclones is inversely correlated with the minimum sea level pressure. Despite fluctuations, the tropical cyclone intensifies in all the simulations. In comparison to the control simulation, NO3, the tropical cyclone in NO9 is stronger before the 72nd hr and is weaker after that, and those in KF9 and HY9 are stronger overall. Some of the variability in the intensity is correlated with the accumulated amount of total precipitation.

In Figure 4.10 (a) and (b), the precipitation in NO9 is more than that in NO3 in the inner regions but is less in the outer regions. This might be caused by the delayed onset of the grid-scale cumulus convection during the low-level inflow, which could probably strengthen the precipitation. However, in Figure 4.11 (a) and (b), the precipitation in NO9 is less than that in NO3 in the eyewall. This might be attributed to the roughened structure of the grid-scale cumulus convection, which could possibly weaken the precipitation. These results hint about the role of cumulus parameterization at 9 km resolution, which should represent the subgrid-scale structure regardless of the presence of the grid-scale cumulus convection.

In Figure 4.10 (c) and (d), some of the difference between HY9 and KF9 could be explained with the effects of local compensation found in the piggyback experiment. For example, the maximum of the total precipitation in KF9 is larger than that in HY9 while the position of that in KF9 is in the outside of that in HY9. This is consistent with the effect of local compensation which increases the precipitation rate in the regions about 30 km outside of the radii of the maximum subgrid-scale precipitation. Moreover, the intensity of the tropical cyclone is generally stronger in KF9 than in HY9. This might be attributed to either the sea level pressure deepening or the precipitation increase due to the local compensation.

Furthermore, considering NO3 as a realistic approximation, the overestimation of the intensity of the tropical cyclone in KF9 is generally reduced in HY9. This might support the conjecture in which the local compensation may be one cause of the tendency of KF at 9 km resolution to overestimate the intensity. Furthermore, the overestimation of the intensity in HY9 might imply other causes, maybe the neglect of σ, of the tendency. However, in Figure 4.11 (c) and (d), the difference between HY9 and KF9 could hardly be explained by the effects of the local compensation. This might be attributed to the nonlinear interaction between cyclone-scale and cumulus-scale processes. Accordingly, the robustness of the conjecture remains in doubt.
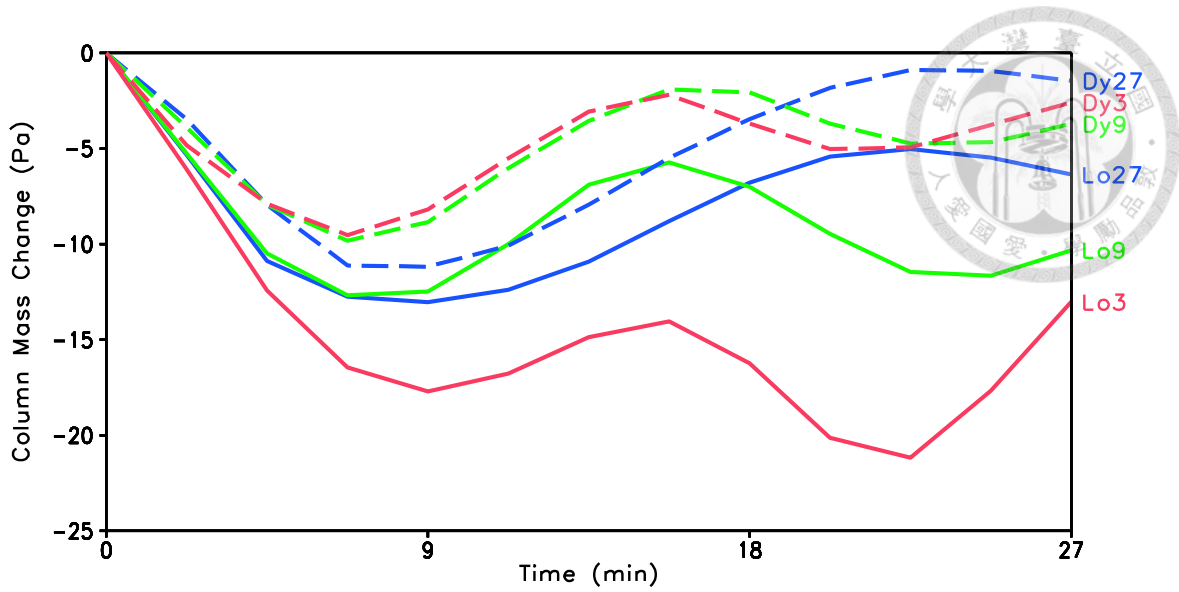
28

Figure 4.1. The temporal evolutions of the column mass change in the mass compensation experiment. Lo denotes the local compensation, and Dy denotes the dynamic compensation. The horizontal resolution of 3, 9, and 27 km, respectively, are used.
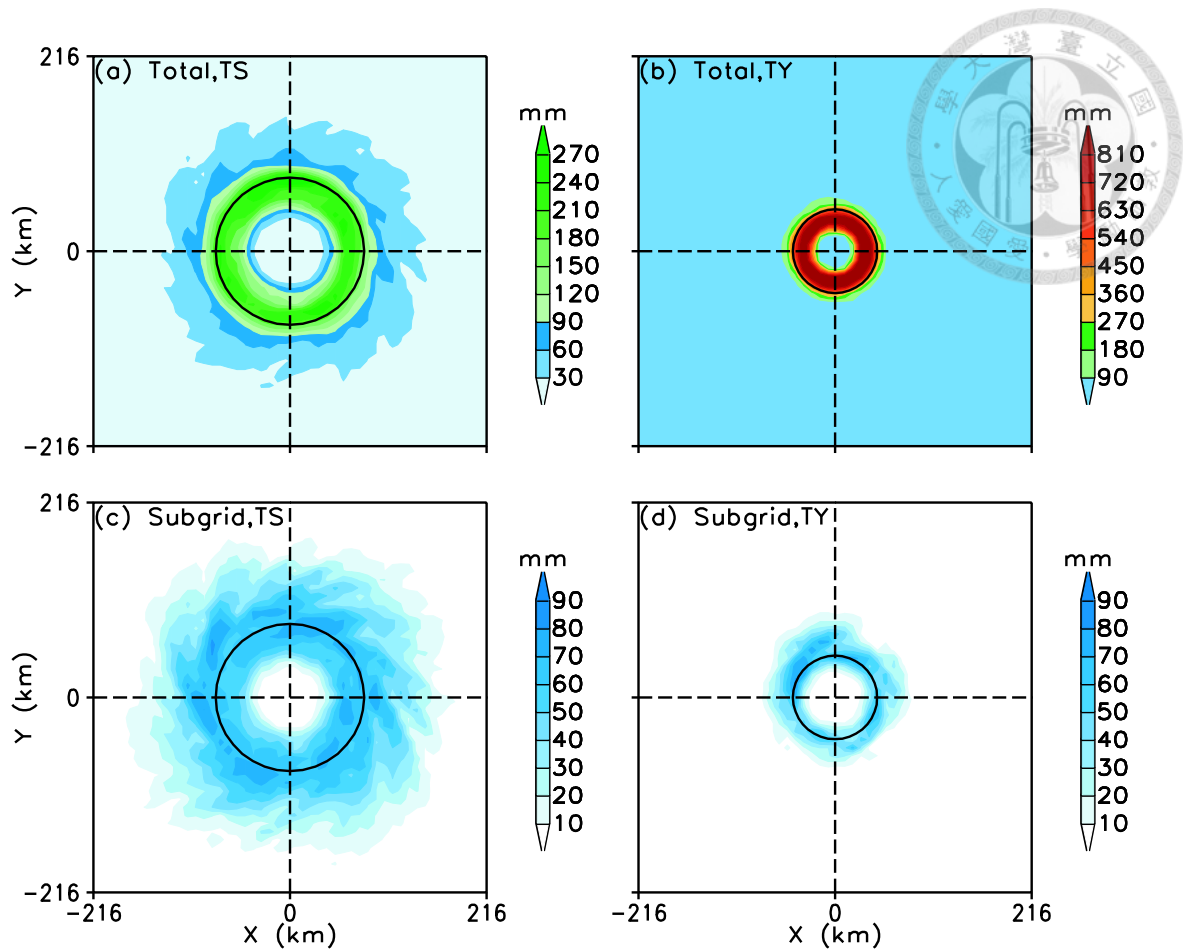
Figure 4.2. The horizontal distributions in the TS stage (left) and in the TY stage (right) in the control simulation in the piggyback experiment of the total precipitation (upper) and the subgrid-scale precipitation (lower). The circles denote the radii of the maximum subgrid-scale precipitation.
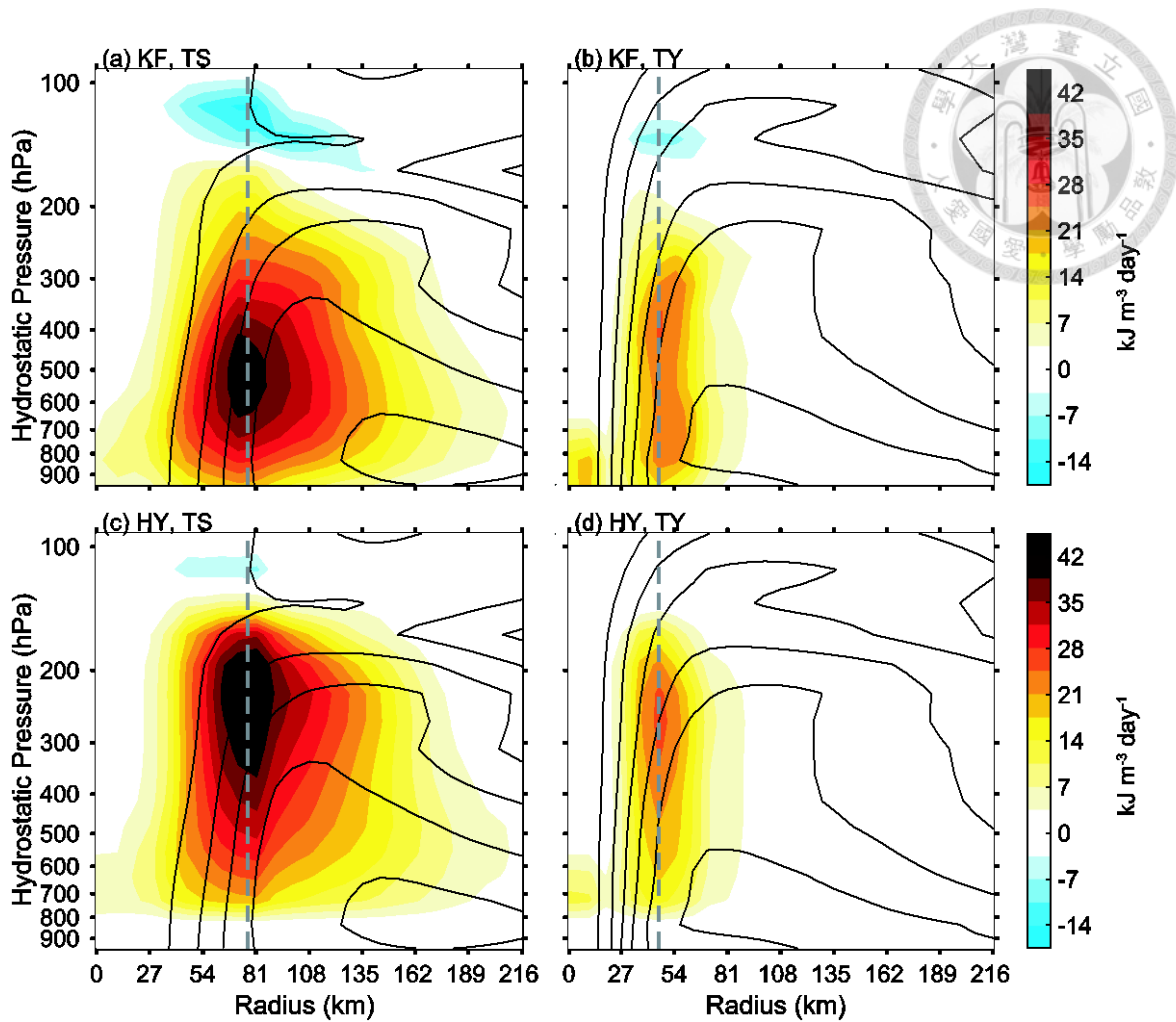
Figure 4.3. The vertical cross sections in the TS stage (left) and in the TY stage (right) in the piggyback experiment of the azimuthal and temporal average of the variables in the following: shaded, subgrid-scale heat sources and sinks with KF (upper) or those plus the subgrid-scale potential energy sources and sinks with HY (lower); and contour, the absolute angular momentum (interval: 5×10^5 m^2 s^{-1}). The dash lines denote the radii of the maximum subgrid-scale precipitation.
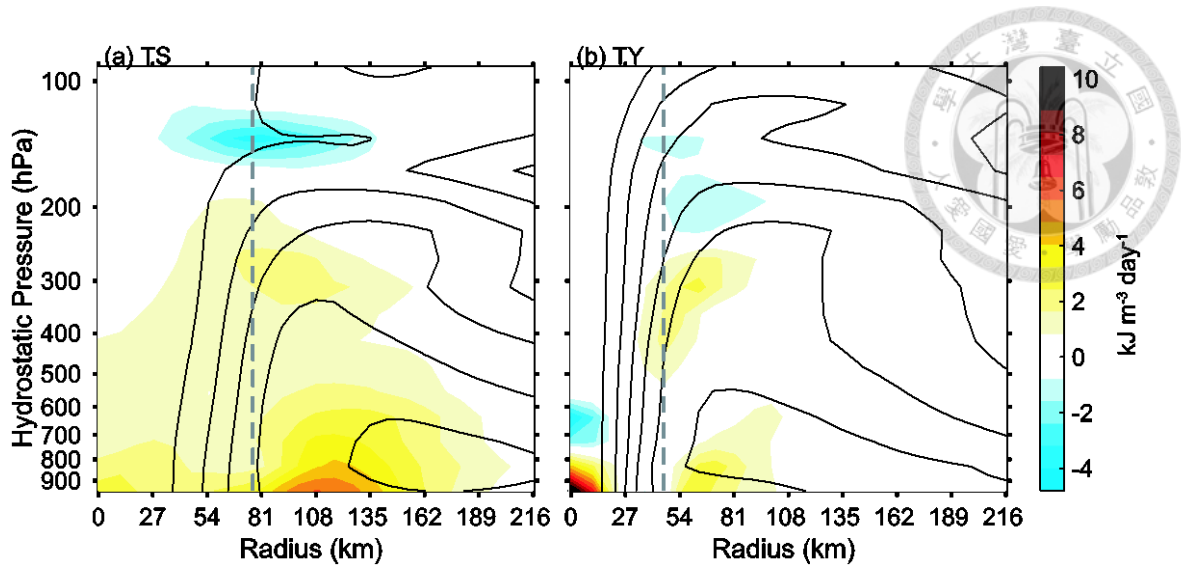
31

Figure 4.4. Similar to Figure 4.3. The colored shades are the enthalpy density change rate due to the local compensation.
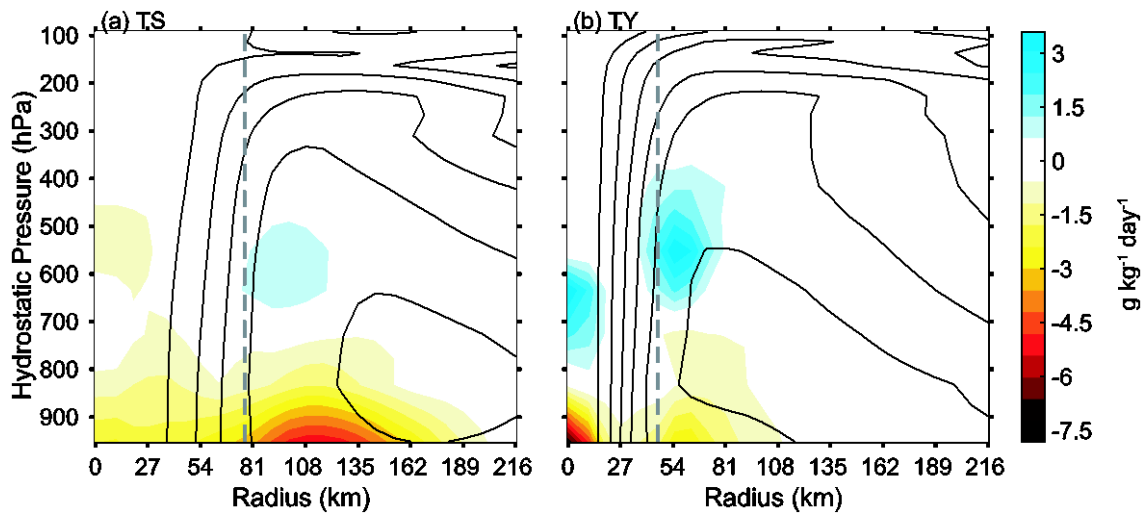

Figure 4.5. Similar to Figure 4.3. The colored shades are the water vapor mixing ratio change rate due to the local compensation.
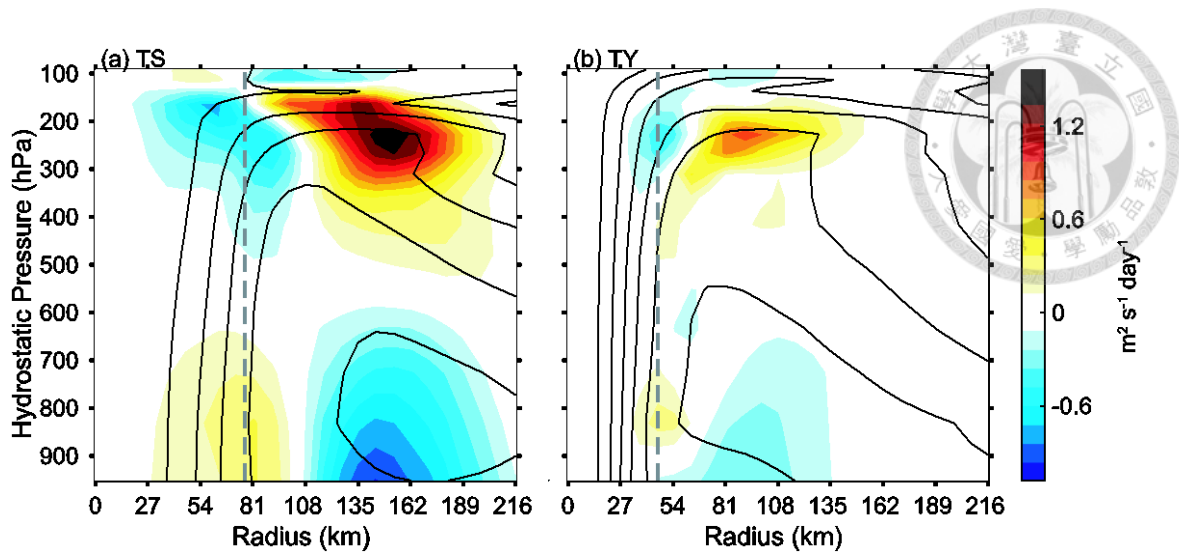
Figure 4.6. Similar to Figure 4.3. The colored shades are the radial mass flux change rate due to the local compensation.
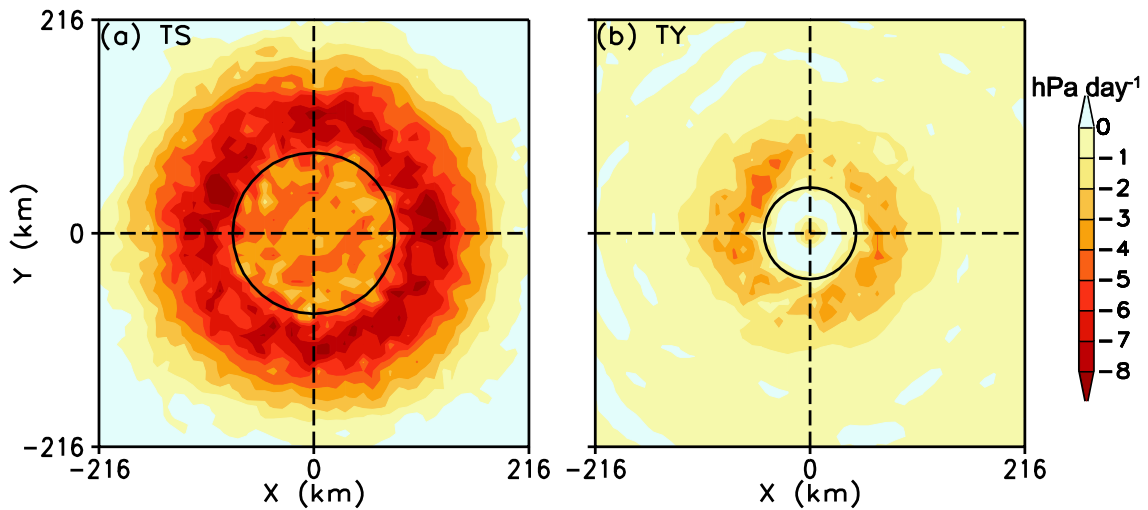

Figure 4.7. The horizontal cross sections in the TS stage (left) and in the TY stage (right) in the piggyback experiment of the temporal average of the sea level pressure change rate due to the local compensation. The circles denote the radii of the maximum subgrid-scale precipitation.
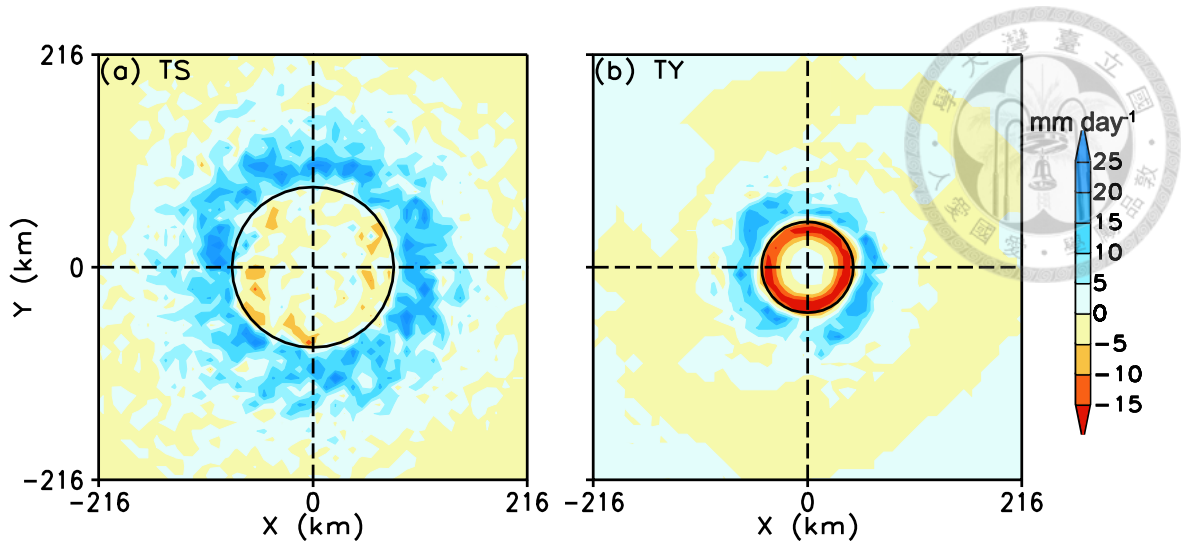
Figure 4.8. Similar to Figure 4.5. The colored shades are the total precipitation change
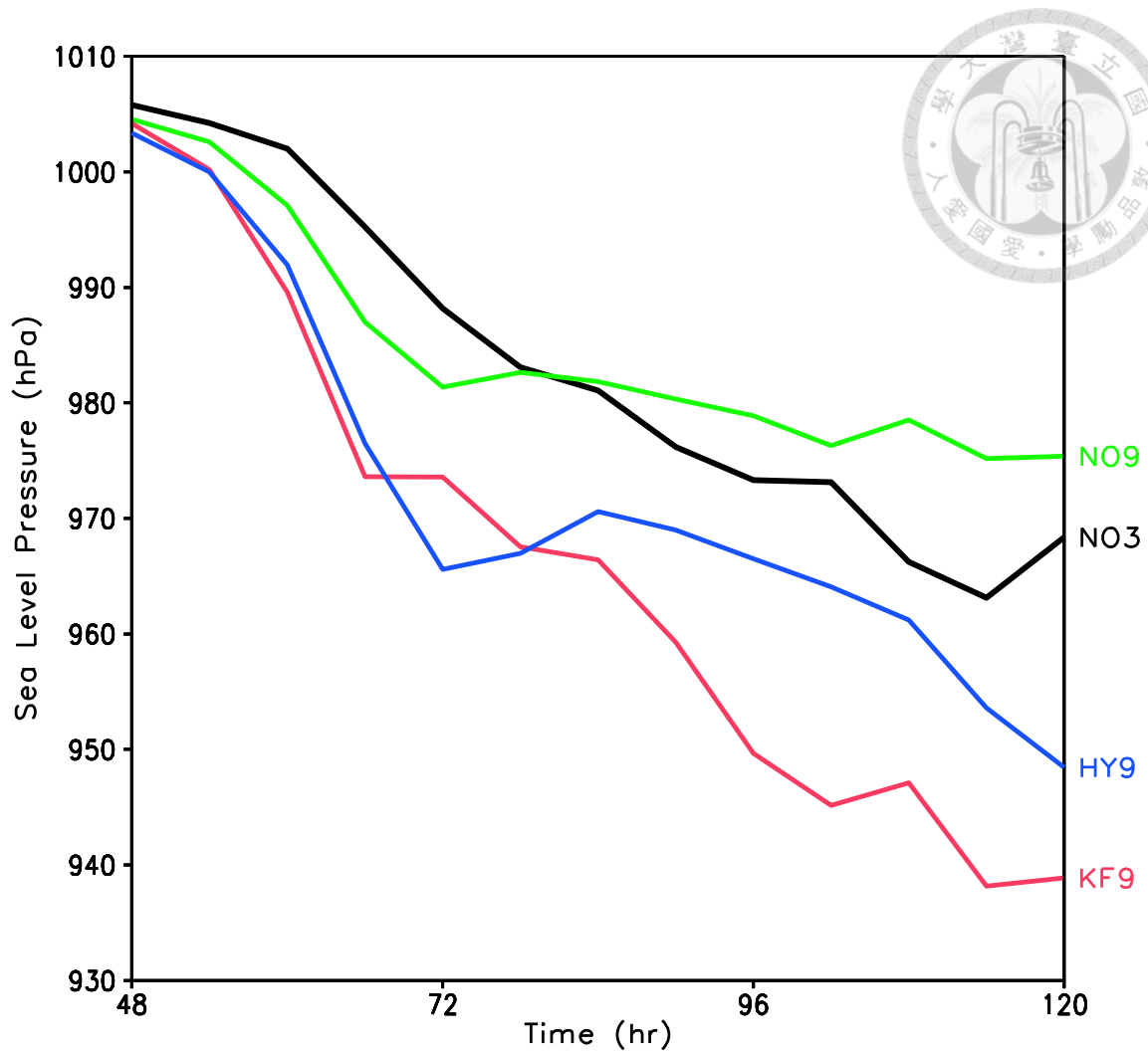
rate due to the local compensation.

Figure 4.9. The temporal evolutions of the minimum sea level pressure in the fully coupled experiment after two-day spin-up. NO3 is the control simulation, at 3 km resolution with the explicit scheme, and NO9, KF9, and HY9 are the sensitivity simulations, at 9 km resolution with the explicit scheme, KF, and HY, respectively.

Figure 4.10. The radial distributions of the azimuthal average of the total precipitation (blue) and the subgrid-scale precipitation (red) in the first 60 hr in the fully coupled experiment. NO3 is the control simulation, at 3 km resolution with the explicit scheme, and NO9, KF9, and HY9 are the sensitivity simulations, at 9 km resolution with 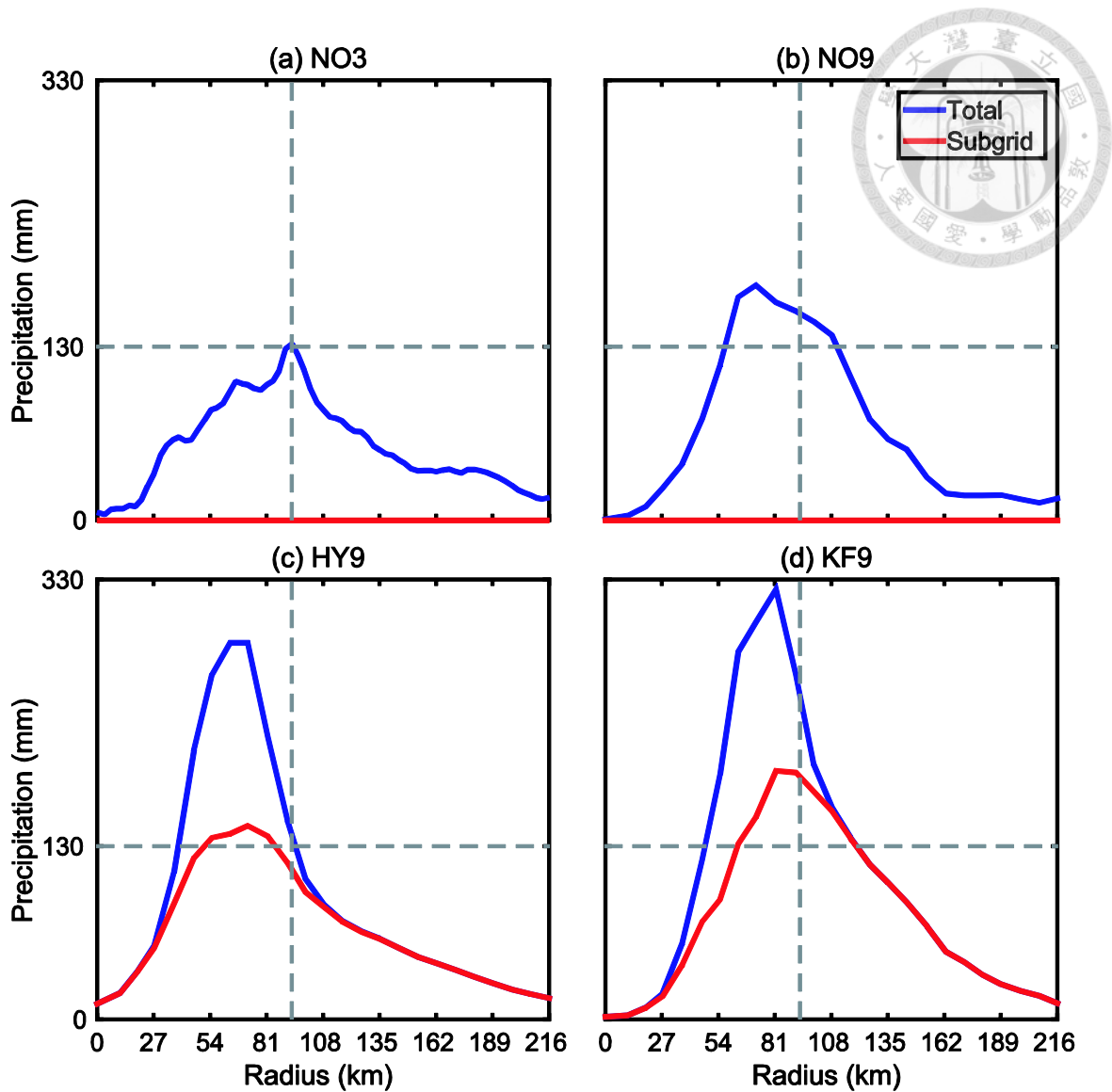the explicit scheme, KF, and HY, respectively. The horizontal and vertical dash lines denote the amount and the location, respectively, of the maximum of total precipitation in NO3.
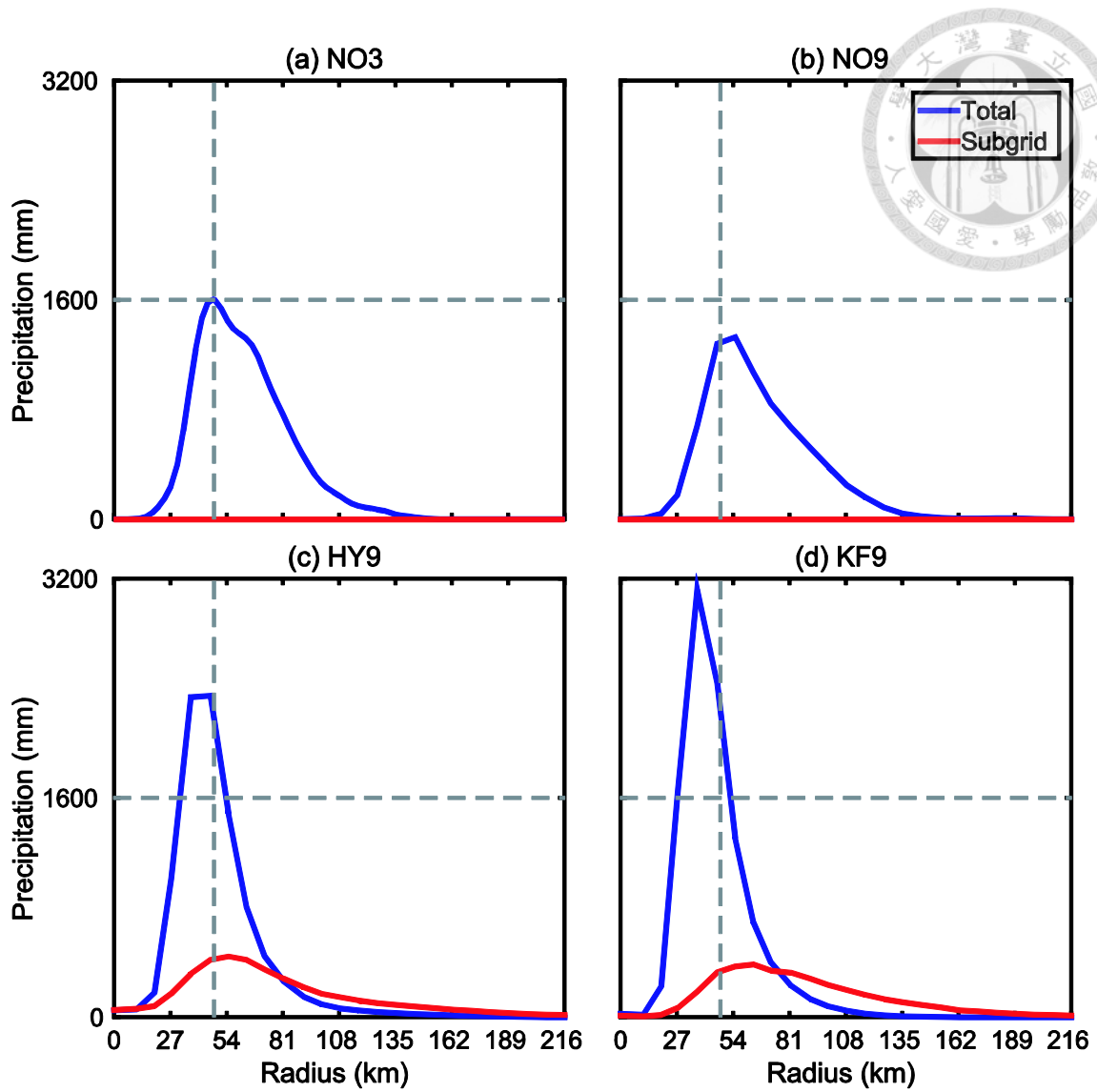
Figure 4.11. Similar to Figure 4.9. The radial distributions of those in the last 60 hr.

5. Conclusions

The dynamic compensation embodies our knowledge in which the mass-compensating motion induced by the subgrid-scale processes could be resolved by the grid-scale ones. With a nonhydrostatic fully compressible continuity equation set, the formulation of hybrid mass flux cumulus schemes (HYMACSs), implementing the dynamic compensation, treats the mass and the other extensive variables in a parallel manner. With the Weather Research and Forecasting Model (WRF), the results of the mass compensation experiment indicate that the dynamic compensation is less sensitive than the local compensation to the horizontal resolution. Considering these and previous studies [*Kuell and Bott*, 2008; *Kuell et al.*, 2007], we conclude that the dynamic compensation is more realistic than the local compensation when formulating cumulus schemes in nonhydrostatic fully compressible models.

On the other hand, the local compensation misrepresents the effects of the subgrid-scale cumulus convection. By subtracting the results with the hybrid mass flux Kain-Fritsch scheme (HY) from those with the Kain-Fritsch scheme (KF) in the piggyback experiment, we infer the effects of the local compensation in a characteristic time of convective adjustment in tropical cyclone simulations at 9 km resolution. The local compensation causes warming and low-level drying and induces a circulation change which could cause other effects, such as sea level pressure deepening and a precipitation increase. The maxima of the effects are as follow: warming, $10.0 \text{ kJ m}^{-3} \text{ day}^{-1}$; low-level drying, $-7.5 \text{ g kg}^{-1} \text{ day}^{-1}$; sea level pressure deepening, $-8.0 \text{ hPa day}^{-1}$; and precipitation strengthening, 25.0 mm day^{-1}. Furthermore, with the explicit scheme at 3 km resolution as a reference, the results of the fully coupled experiment support that the local compensation might be a cause of the tendency of KF at 9 km resolution to

38

overestimate the intensity of simulated tropical cyclones, but there is uncertainty due to the nonlinear interaction between cyclone-scale and cumulus-scale processes.
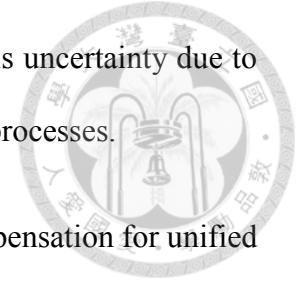
Here we discuss the importance of eliminating the local compensation for unified cumulus parameterization problem. A hierarchy of cumulus schemes from particular ones to general ones could be built according to the scheme formulation in section 2. By eliminating the assumptions one by one, the hierarchy with six levels should be built as follows:

Level 1, the conventional cumulus schemes. Assume the local compensation, the neglect of σ, the steady state, the top-hat profile, and the ensemble-spatial-temporal average.

Level 2, the HYMACSs. Eliminate the local compensation by the dynamic compensation, so the mass-compensating motion is resolved.

Level 3. Eliminate the neglect of σ by parameterizing σ, so the convective drafts could be partially resolved.

Level 4. Eliminate the steady state by prognostic closures, so the convective drafts could interact with grid-scale changes which are faster than the convective adjustment.

Level 5. Use a more complex profile than the top-hat profile, so the structure within the convective drafts or within the clear sky could be considered.

Level 6. No longer treat the ensemble average as the spatial average in a grid box, so the problem could be considered in a continuous space.

Most of the assumptions should be replaced by more sophisticated ones except the local compensation, whose elimination simplifies the scheme formulation in a parallel manner.

The unified cumulus parameterization should be developed following the hierarchy level by level. If a higher level is built before a lower level, the higher level

might be based on a particular artificial assumption which should be eliminated in the lower level. This could be a serious problem when the assumption causes significant effects. Consequently, the elimination of the local compensation should be urgent for the development of the unified cumulus parameterization problem.
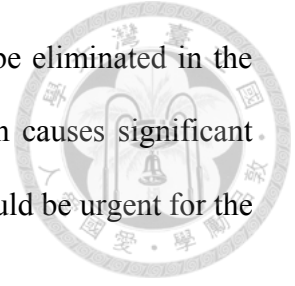
References
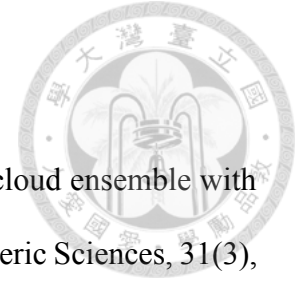
Arakawa, A., and W. H. Schubert (1974), Interaction of a cumulus cloud ensemble with the large-scale environment, Part I, Journal of the Atmospheric Sciences, 31(3), 674-701, doi: 10.1175/1520-0469(1974)031<0674:IOACCE>2.0.CO;2.

Arakawa, A., and C.-M. Wu (2013), A unified representation of deep moist convection in numerical modeling of the atmosphere. Part I, Journal of the Atmospheric Sciences, 70(7), 1977-1992, doi: 10.1175/JAS-D-12-0330.1.

Arakawa, A., J.-H. Jung, and C.-M. Wu (2011), Toward unification of the multiscale modeling of the atmosphere, Atmospheric Chemistry and Physics, 11(8), 3731-3742, doi: 10.5194/acp-11-3731-2011.

Beljaars, A. (1995), The parametrization of surface fluxes in large-scale models under free convection, Quarterly Journal of the Royal Meteorological Society, 121(522), 255-270, doi: 10.1002/qj.49712152203.

Chandrasekar, R., and C. Balaji (2012), Sensitivity of tropical cyclone Jal simulations to physics parameterizations, Journal of earth system science, 121(4), 923-946, doi: 10.1007/s12040-012-0212-8.

Dyer, A., and B. Hicks (1970), Flux-gradient relationships in the constant flux layer, Quarterly Journal of the Royal Meteorological Society, 96(410), 715-721, doi: 10.1002/qj.49709641012.

Emanuel, K. A. (1991), A scheme for representing cumulus convection in large-scale models, Journal of the Atmospheric Sciences, 48(21), 2313-2329, doi: 10.1175/1520-0469(1991)048<2313:ASFRCC>2.0.CO;2.

Gregory, D., and P. Rowntree (1990), A mass flux convection scheme with representation of cloud ensemble characteristics and stability-dependent closure, Monthly

Weather Review, 118(7), 1483-1506, doi: 10.1175/1520-0493(1990)118<1483:AMFCSW>2.0.CO;2.
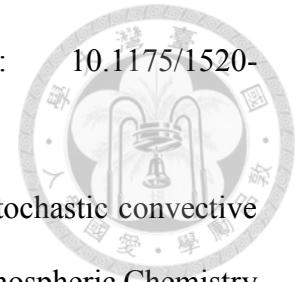
Grell, G. A., and S. R. Freitas (2014), A scale and aerosol aware stochastic convective parameterization for weather and air quality modeling, Atmospheric Chemistry and Physics, 14(10), 5233-5250, doi: 10.5194/acpd-13-23845-2013.

Haghroosta, T., W. Ismail, P. Ghafarian, and S. Barekati (2014), The efficiency of the WRF model for simulating typhoons, Natural Hazards and Earth System Sciences Discussions, 2, 287-313, doi: 10.5194/nhessd-2-287-2014.

Hong, S.-Y., Y. Noh, and J. Dudhia (2006), A new vertical diffusion package with an explicit treatment of entrainment processes, Monthly Weather Review, 134(9), 2318-2341, doi: 10.1175/MWR3199.1.

Kain, J. S. (2004), The Kain-Fritsch convective parameterization: an update, Journal of Applied Meteorology, 43(1), 170-181, doi: 10.1175/1520-0450(2004)043<0170:TKCPAU>2.0.CO;2.

Kain, J. S., and J. M. Fritsch (1990), A one-dimensional entraining/detraining plume model and its application in convective parameterization, Journal of the Atmospheric Sciences, 47(23), 2784-2802, doi: 10.1175/1520-0469(1990)047<2784:AODEPM>2.0.CO;2.

Kain, J. S., and J. M. Fritsch (1993), Convective parameterization for mesoscale models: The Kain-Fritsch scheme, in The representation of cumulus convection in numerical models, edited, pp. 165-170, Springer.

Kessler, E. (1995), On the continuity and distribution of water substance in atmospheric circulations, Atmospheric research, 38(1), 109-145, doi: 10.1016/0169-8095(94)00090-Z.

Kuell, V., and A. Bott (2008), A hybrid convection scheme for use in non-hydrostatic numerical weather prediction models, Meteorologische Zeitschrift, 17(6), 775-783, doi: 10.1127/0941-2948/2008/0342.
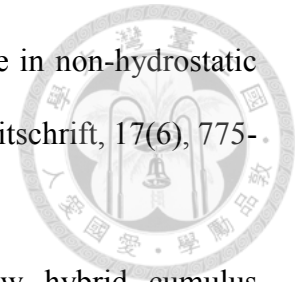
Kuell, V., A. Gassmann, and A. Bott (2007), Towards a new hybrid cumulus parametrization scheme for use in non-hydrostatic weather prediction models, Quarterly Journal of the Royal Meteorological Society, 133(623), 479-490, doi: 10.1002/qj.28.

Molinari, J., and M. Dudek (1992), Parameterization of convective precipitation in mesoscale numerical models: A critical review, Monthly Weather Review, 120(2), 326-344, doi: 10.1175/1520-0493(1992)120<0326:POCPIM>2.0.CO;2.

Park, S. (2014), A unified convection scheme (UNICON). Part I: Formulation, Journal of the Atmospheric Sciences, 71(11), 3902-3930, doi: 10.1175/JAS-D-13-0233.1.

Paulson, C. A. (1970), The mathematical representation of wind speed and temperature profiles in the unstable atmospheric surface layer, Journal of Applied Meteorology, 9(6), 857-861, doi: 10.1175/1520-0450(1970)009<0857:TMROWS>2.0.CO;2.

Rotunno, R., and K. A. Emanuel (1987), An air-sea interaction theory for tropical cyclones. Part II: Evolutionary study using a nonhydrostatic axisymmetric numerical model, Journal of the Atmospheric Sciences, 44(3), 542-561, doi: 10.1175/1520-0469(1987)044<0542:AAITFT>2.0.CO;2.

Sing, K. S., and M. Mandal (2014), Sensitivity of Mesoscale Simulation of Aila Cyclone to the Parameterization of Physical Processes Using WRF Model, in Monitoring and Prediction of Tropical Cyclones in the Indian Ocean and Climate Change, edited, pp. 300-308, Springer.

Skamarock, W., J. Klemp, J. Dudhia, D. Gill, D. Barker, M. Duda, X. Huang, W. Wang, and J. Powers (2008), A description of the Advanced Research WRF Version 3, NCAR technical note, Mesoscale and Microscale Meteorology Division, National Center for Atmospheric Research, Boulder, Colorado, USA.

Srinivas, C., R. Venkatesan, D. B. Rao, and D. H. Prasad (2007), Numerical simulation of Andhra severe cyclone (2003): Model sensitivity to the boundary layer and convection parameterization, in Atmospheric and Oceanic, edited, pp. 1465-1487, Springer.

Sun, Y., L. Yi, Z. Zhong, Y. Hu, and Y. Ha (2013), Dependence of model convergence on horizontal resolution and convective parameterization in simulations of a tropical cyclone at gray-zone resolutions, Journal of Geophysical Research: Atmospheres, 118(14), 7715-7732, doi: 10.1002/jgrd.50606.

Tiedtke, M. (1989), A comprehensive mass flux scheme for cumulus parameterization in large-scale models, Monthly Weather Review, 117(8), 1779-1800, doi: 10.1175/1520-0493(1989)117<1779:ACMFSF>2.0.CO;2.

Webb, E. K. (1970), Profile relationships: The log-linear range, and extension to strong stability, Quarterly Journal of the Royal Meteorological Society, 96(407), 67-90, doi: 10.1002/qj.49709640708.

Wu, C.-M., and A. Arakawa (2014), A unified representation of deep moist convection in numerical modeling of the atmosphere. Part II, Journal of the Atmospheric Sciences, 71(6), 2089-2103, doi: 10.1175/JAS-D-13-0382.1.

Zhang, D., and R. A. Anthes (1982), A high-resolution model of the planetary boundary layer-sensitivity tests and comparisons with SESAME-79 data, Journal of Applied Meteorology, 21(11), 1594-1609, doi: 10.1175/1520-0450(1982)021<1594:AHRMOT>2.0.CO;2.

Zhang, G. J., and N. A. McFarlane (1995), Sensitivity of climate simulations to the parameterization of cumulus convection in the Canadian Climate Centre general circulation model, Atmosphere-ocean, 33(3), 407-446, doi: 10.1080/07055900.1995.9649539.

Zheng, Y., K. Alapaty, J. A. Herwehe, A. D. Del Genio, and D. Niyogi (2015), Improving High-Resolution Weather Forecasts using the Weather Research and Forecasting (WRF) Model with an Updated Kain-Fritsch Scheme, Monthly Weather Review(2015), doi: 10.1175/MWR-D-15-0005.1.